Progress in Natural Science: Materials International 2013;23(4):434–439

Chinese Materials Research Society

Progress in Natural Science: Materials International

www.elsevier.com/locate/pnsmi
www.sciencedirect.com

# Structure evolution of $Y_2O_3$ nanoparticle/Fe composite during mechanical milling and annealing

**Tong Liu[a,*], Hailong Shen[a], Chenxi Wang[a], Wusheng Chou[b]**

[a]*Key Laboratory of Aerospace Materials and Performance (Ministry of Education), School of Materials Science and Engineering, Beihang University, Beijing 100191, China*
[b]*School of Mechanical Engineering and Automation, Beihang University, Beijing 100191, China*

Received 31 December 2012; accepted 29 May 2013
Available online 18 July 2013

**KEY WORDS**

$Y_2O_3$ nanoparticles;
Oxide dispersion strengthened composite;
Mechanical milling;
Amorphous structure

**Abstract** Fe-25 wt% $Y_2O_3$ composite powders have been fabricated by mechanical milling (MM) Fe powders of 100 μm in diameter and $Y_2O_3$ nanoparticles in an argon atmosphere for the milling periods of 4, 8, 12, 24, 36, and 48 h, respectively. The features of these powders were characterized by using X-ray diffraction (XRD), scanning electron microscopy (SEM), electron probe micro analyzer (EPMA) and transmission electron microscopy (TEM). The experimental results showed that the mean particle size and crystalline size of MM powders decreased with the milling time increasing. All the elements distributed homogenously inside the powders after 48 h of MM. The lattice constant of the matrix α-Fe kept constant with the milling time, and no solid solution took place during MM process. After 8 h of MM, the α-Fe in each powder became nanocrystalline. After 48 h of MM, $Y_2O_3$ changes from nanostructure into amorphous structure, and the crystalline size of α-Fe further decreased to 10 nm. The $Y_2O_3$ in the powders mechanically milled for 48 h kept the amorphous structure after being annealed at 400 °C, and starts to crystallize when the powders are annealed at 600 °C. The amorphous $Y_2O_3$ contains a small amount of Fe, and crystalline $FeYO_3$ appears at 800 °C.



## 1. Introduction

It is well known that oxide with a low solubility in metals is difficult to be evenly dispersed in a metal matrix via conventional processes, such as melting and casting [1,2]. In the late 1960s, Benjamin et al. [3,4] firstly developed the epoch-making MM process and successfully produced oxide-dispersion strengthened (ODS) superalloys for high temperature applications. This novel solid state process enables the insoluble refractory oxide particles

*Corresponding author. Tel./fax: +86 10 8231 6192.
E-mail address: tongliu@buaa.edu.cn (T. Liu).
Peer review under responsibility of Chinese Materials Research Society.

Production and hosting by Elsevier

1002-0071 © 2013 Chinese Materials Research Society. Production and hosting by Elsevier B.V. All rights reserved.
http://dx.doi.org/10.1016/j.pnsc.2013.06.009

to be finely and homogeneously distributed in the metal matrix. The uniform dispersion of nanoscale and thermo-stable oxide particles inhibits dislocation motion and strengthens the metal matrix. Due to their excellent strength and exceptional creep resistance, ODS alloys have been utilized in the areas, including aerospace, thermal processing and glass processing industries [5–7]. Recently, ODS ferritic steel with excellent irradiation resistance also becomes one of the most promising candidates for the blanket structures in the nuclear power plants [8–10].

The chemical and physical properties of the dispersoids are of great importance in fulfilling their functions in ODS alloys. Generally, they should possess a high melting point and a low solubility and diffusion rate in the matrix in order to keep chemical and size stability at high temperature [4]. Among various oxides such as $Al_2O_3$, $ThO_2$ and $La_2O_3$, yttria has been widely adopted as the dispersoid in ODS alloys as the result of its outstanding dimensional and structural stability even up to 1300 °C [11]. Munoz-Morris et al. [12] prepared ODS Fe–40Al containing about 1 vol% $Y_2O_3$ by MM. The room temperature yield strength of Fe–40Al containing nanocrystalline oxide particles is as high as 1092 MPa. Miodownik et al. [13] examined the microstructure of ODS Ni-base superalloy and proposed the possible mechanisms for the triggering of secondary recrystallization as well as the origin of the strong annealing texture in the extruded MA754. In the past 30 years, many interests have been focused on the mechanical properties and the matrix microstructures of various ODS alloys (e.g. Ni, Fe, Cu and Co-base alloys) [14–18] and intermetallics (FeAl and NiAl) [19,20]. It should be noted that the size and structural evolution of oxide particles during MM and subsequent consolidation process are very important to tailor the microstructure and properties of ODS alloys. Nevertheless, the morphology and structural change of the $Y_2O_3$ particles during MM processing has not been comprehensively investigated.

Some researchers suggested the possibility of oxide powder being not only finely divided but also decomposed in the metal matrix [21,22]. Kimura et al. [21] investigated the microstructural changes of Fe–24Cr-15 wt% $Y_2O_3$ during MM. They pointed out that concerning the dissolution of $Y_2O_3$ during mechanical milling, $Y_2O_3$ particles almost decomposed to form amorphous grain boundary layer where Y and O atoms are enriched. On the other hand, they also argued that $Y_2O_3$ particles almost decomposed and dissolved into the matrix, and the fine $Y_2O_3$ reprecipitated after annealing [21]. Okuda et al. [22] argued that $Y_2O_3$ decomposed to yttrium and oxygen atoms during the MM process and dissolved in the 13% Cr ferritic steel. Therefore, it is necessary to clarify whether $Y_2O_3$ particles decomposed, dissolved and reprecipitated or they form amorphous structure and then crystallize during the subsequent heat treatment. Moreover, the detailed information concerning the oxide microstructure evolution is still very limited. The knowledge of oxide particles and their status within the matrix will help us understand the strengthening mechanism of ODS alloys. In this study, we adopt a simple system, Fe-25 wt% $Y_2O_3$, as a model alloy in order to clarify the morphology change and structural evolution of yttria during MM and subsequent annealing.

## 2. Experimental

The purities of Fe and $Y_2O_3$ particles are 99.9%. The mean particle size of raw Fe powders is about 100 μm. The raw $Y_2O_3$ nanoparticles are in the shape of nano-rod, with a diameter of about 20 nm and a length of about 100 nm, see Fig. 1. Fe-25 wt% $Y_2O_3$ powders were mechanically milled by a planetary ball mill with ball to power ratio of 15:1 at a rotation speed of 300 rpm in Ar atmosphere (99.999%) for 4, 8, 12, 24, 36 and 48 h, respectively. The crystal structures of the powders mechanically milled for different lengths of time were characterized by using a Rigaku X-ray diffractometer (XRD) with monochromatic Cu Kα radiation. The crystal structures of the powders mechanically milled for 48 h were also characterized in-situ at different temperatures by using a Rigaku XRD with monochromatic Co Kα radiation. The particle size, morphology and composition were investigated by scanning electron microscope (SEM) and electron probe micro-analyzer (EPMA). Transmission electron microscopy (TEM) and selected area electron diffraction (SAED) were used to investigate the microstructures of the particles mechanically milled for 8 h and 48 h with JEOL-JSM-2100F at an accelerating voltage of 200 kV. Thermogravimetry-differential thermal analysis (TG-DTA) of the powders mechanically milled for 48 h was carried out between room temperature and 1200 °C at a heating rate of 10 °C/min and in flowing Ar of 400 ml/min.

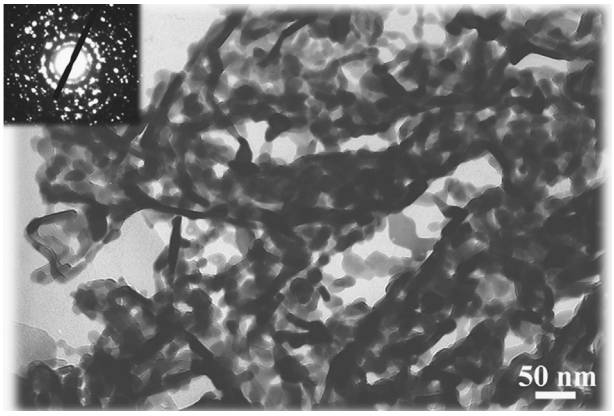


**Fig. 1** TEM bright field image and in-set SAED pattern of raw $Y_2O_3$ particles.

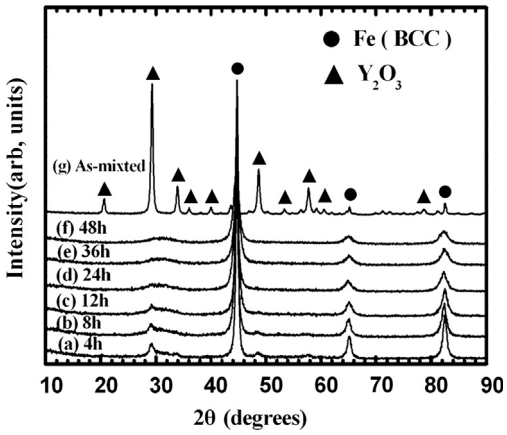


**Fig. 2** XRD patterns of Fe-25 wt% $Y_2O_3$ powders mechanically milled for (a) 4, (b) 8, (c) 12, (d) 24, (e) 36, (f) 48 h and (g) as mixed.

## 3. Results and discussion

Fig. 2 shows the XRD patterns of Fe-25 wt% $Y_2O_3$ powder samples after being milled for different lengths of time. It can be

seen from Fig. 2(g) that the iron and $Y_2O_3$ mixture before MM exhibits the diffraction peaks of both α-Fe and $Y_2O_3$. The intensities of these diffraction peaks decrease and broaden with increasing milling time. This is mainly attributed to the decrease of crystalline size caused by MM. It was also found in Fig. 2 that with an increase of milling time, the diffraction peaks of α-Fe do not show any shifting. This confirms that few yttrium and oxygen atoms dissolve into the α-Fe crystalline lattice during MM. The diffraction peaks at about 20.2°, 34.0°, 35.9°, 39.9°, 53.2°, 57.6°, 60.5° and 78.8° of $Y_2O_3$ disappear after 4 h of MM. As the milling time increases, the diffraction peaks of $Y_2O_3$ gradually broaden. After 24 h of MM, only the very weak peak around 30° can be detected. It is worth to note that after 48 h of MM, $Y_2O_3$ in the MM powder only displays a broad diffuse peak between 28° and 34°, indicating the formation of amorphous structure. This phenomenon has not been found in the common ODS alloys due to their low contents of $Y_2O_3$ (about 0.3–1.0 wt%) and the difficulty to identify the formation of amorphous structure via XRD analysis [23,24]. It is reported that many alloys and oxides systems have the trend to form amorphous structure during MM, such as the M–Si (M = Ni, Co, Mo, Mn, and Cr) [25], Ag–Pd [26] and $ZrO_2$–$Fe_2O_3$ [27] systems. Omuro et al. [25] reported that $Ni_{70}Si_{30}$ changes into amorphous structure after 132 h of milling. Jiang et al. [27] reported that 20 mol% α-$Fe_2O_3$-80 mol% $ZrO_2$ formed amorphous structure after 42 h of milling. It is proposed that Fe also plays important roles in the amorphization of $Y_2O_3$. The Fe particles with good plastic deformation capacity promote the crushing behavior of $Y_2O_3$ particles by separating them apart during MM. Moreover, a small amount of Fe atoms may also enter the lattice of $Y_2O_3$ and cause the lattice distortion, which accelerates the amorphization of $Y_2O_3$. This will be proved by the in-situ XRD analysis during annealing hereafter.

Fig. 3 shows the cross section SEM images of Fe-25 wt% $Y_2O_3$ powders mechanically milled for 8 h and 48 h. The cross sections of the powders being mechanically milled for 8 h show irregular shapes, and the particle size ranges from 1 to 40 μm with an average of about 4 μm, see Fig. 3(a). This is ascribed to the severe plastic deformation during MM. The matrix metal of iron gets work-hardening and is broken into small particles, while the brittle $Y_2O_3$ nanoparticles are broken further by the mechanical collisions, which is proved by EPMA analysis hereafter. Fig. 3(b) shows that the size of the powders mechanically milled for 48 h is remarkably decreased, and the average particle size is about 2 μm with a narrow size distribution between 1 and 10 μm. Moreover, Fig. 3 shows that the particle shape gradually changes from irregular shape after 8 h of MM into nearly spherical shape after 48 h of MM. Dai et al. [28] studied the Fe–9Cr-15 wt% $Y_2O_3$ powders after mechanically milling for various periods. They found that the mean particle sizes of the powder samples are 40 μm, 10 μm and 3 μm after being milled for 10 h, 30 h and 56 h, respectively, which are relatively larger than those of Fe-25 wt% $Y_2O_3$ powders milled for the same periods. We suppose that this is due to the different compositions between these two alloys. The EPMA element mapping analysis of the selected areas in Fig. 3 is presented in Fig. 4. It is apparently found in Fig. 4(a) that the elements of Fe, O and Y are not distributed evenly inside the powder milled for 8 h, implying that 8 h of MM are not long enough to mix all the elements in the powder homogeneously. On the other hand, it is clear that all the elements (Fe, O and Y) are distributed evenly inside one powder milled for 48 h, as seen in Fig. 4(b), which demonstrates that $Y_2O_3$ nanoparticles are further broken into smaller size during MM. It is concluded that the brittle $Y_2O_3$ nanoparticles are broken further by the mechanical collisions and the milling of Fe and $Y_2O_3$ powders reaches a saturation state in 48 h, which is consistent with the XRD results.

Fig. 5 shows the TEM image and the corresponding SAED pattern of one typical Fe-25 wt% $Y_2O_3$ powder milled for 8 h. The size of the particle is about 400 nm in diameter. The TEM image exhibits a complicated contrast. It is difficult to determine the crystalline grain size of the matrix directly from the bright field TEM image. It can be confirmed from the SAED pattern in Fig. 5 (b) that the powder is polycrystalline, and diffraction rings related to $Y_2O_3$ (222) and α-Fe (110) were detected. Since the particle diameter is only 400 nm, it is deduced that the powder is made of many nanocrystals including the nanocrystal $Y_2O_3$ that distributed in the matrix of the nanocrystal α-Fe. Fig. 6 shows the TEM image and the corresponding SAED pattern of a typical Fe-25 wt% $Y_2O_3$ powder after being mechanically milled for 48 h. The size of the particle is about 300 nm in diameter. Compared with Fig. 5, Fig. 6 (a) shows quite uniform contrast, implying that $Y_2O_3$ are evenly dispersed in α-Fe. It can be seen from Fig. 6(b) that three outer rings belong to Fe (110), Fe (200) and Fe (211), respectively. These rings are made of continuous diffraction spots, indicating that the crystalline size is further decreased. From the SAED pattern of α-Fe rings, it can be also deduced that there are a lot of α-Fe grains in nanoscale with random crystallographic orientations within one particle. An inner halo ring can be detected in Fig. 6(b). By calculating the radius of this halo ring, it is suggested that this halo ring belongs to the amorphous $Y_2O_3$.

Fig. 7 shows a HRTEM image of the Fe-25 wt% $Y_2O_3$ powder milled for 48 h. In the "a" areas of Fig. 7, the lattice fringes are clearly observed, which can be indexed to the lattice planes

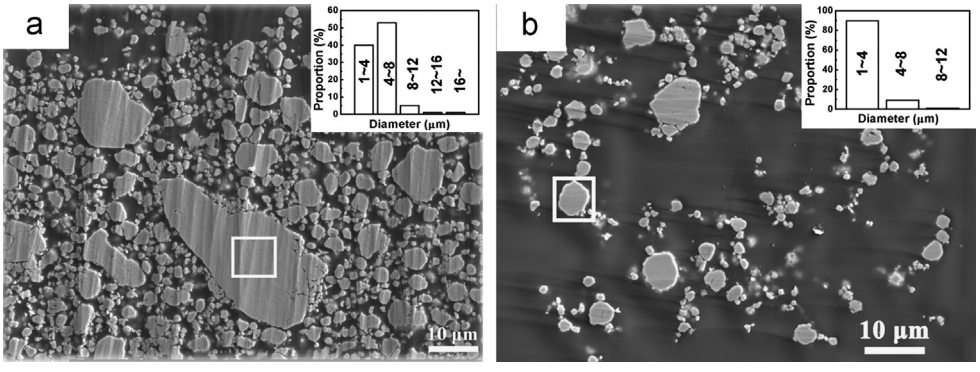


**Fig. 3** Cross section SEM images of Fe-25 wt% $Y_2O_3$ powders mechanically milled for (a) 8 and (b) 48 h.

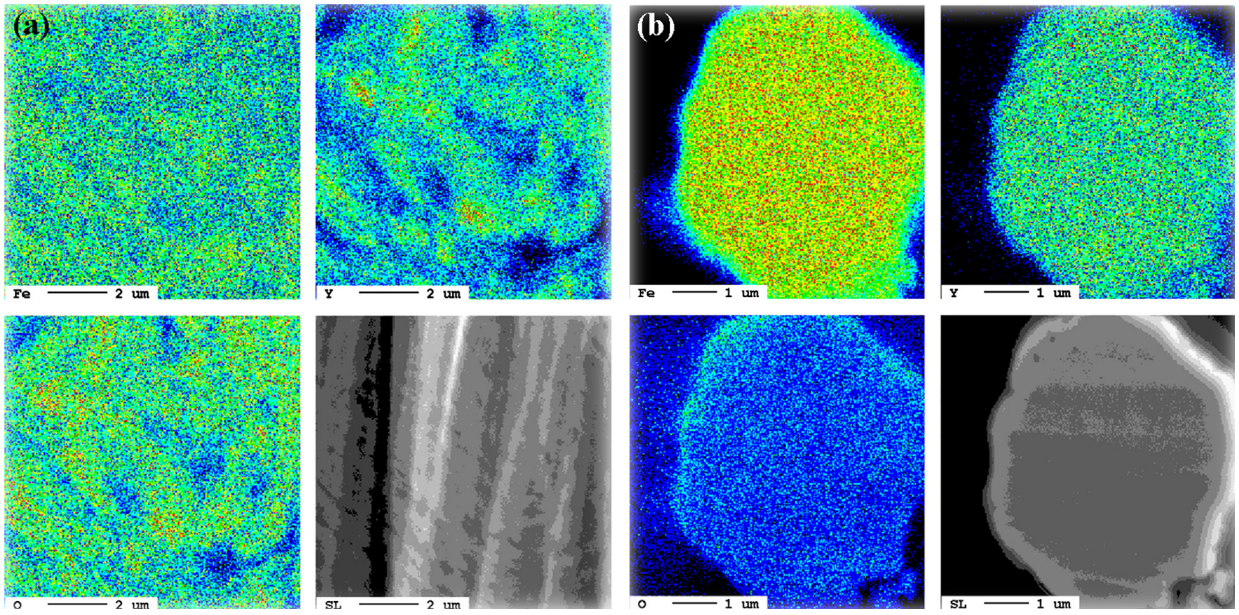


**Fig. 4** Cross section element mapping by EPMA of Fe-25 wt% $Y_2O_3$ powders mechanically milled for (a) 8 and (b) 48 h.

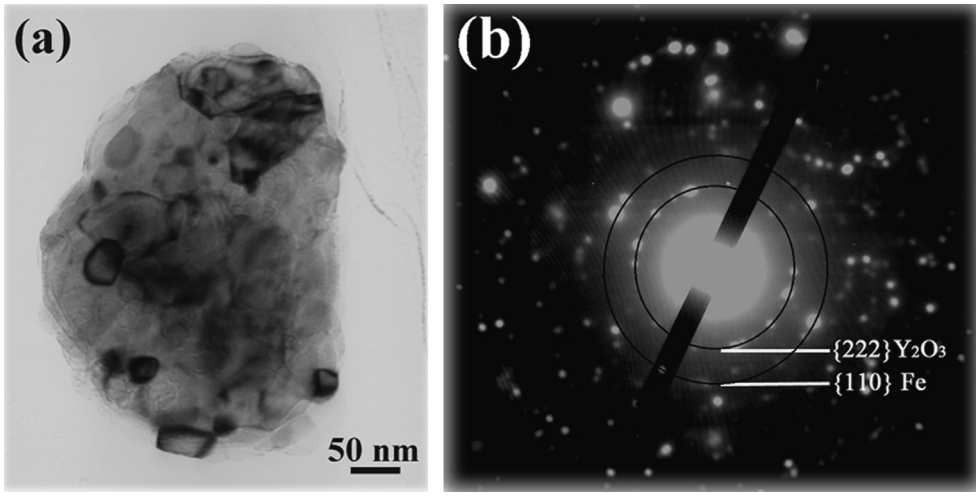


**Fig. 5** TEM bright field image and SAED pattern of one typical Fe-25 wt% $Y_2O_3$ powder milled for 8 h.

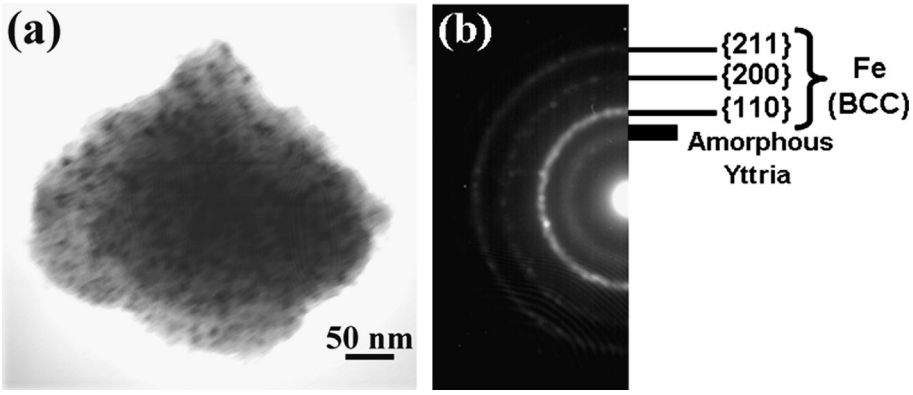


**Fig. 6** TEM bright field image and SAED pattern of one typical Fe-25 wt% $Y_2O_3$ powder milled for 48 h.

of α-Fe (110) on the basis of their lattice spacings. This also demonstrates the nanocrystalline structure of the matrix α-Fe with a grain size of 10 nm. In the "b" area of Fig. 7, no lattice fringes are detected, indicating that the amorphous $Y_2O_3$ is situated at the grain boundaries of α-Fe. Thus, it is concluded that the nanostructure of Fe derived from MM offers a large amount of grain

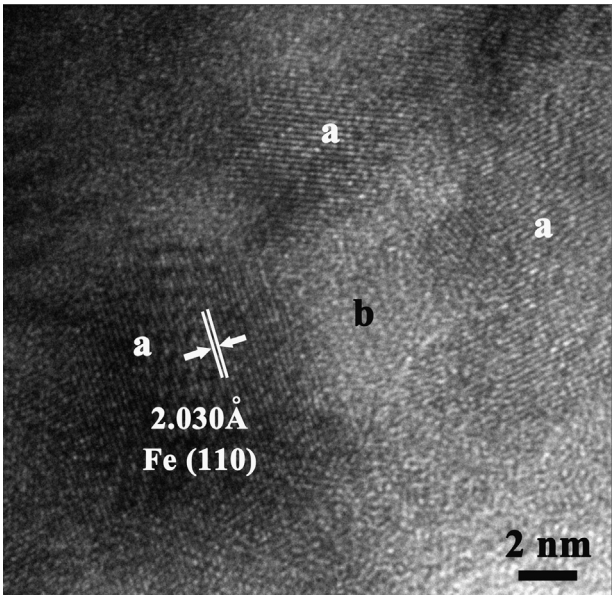


**Fig. 7** HRTEM bright field image of a Fe-25 wt% $Y_2O_3$ powder milled for 48 h.

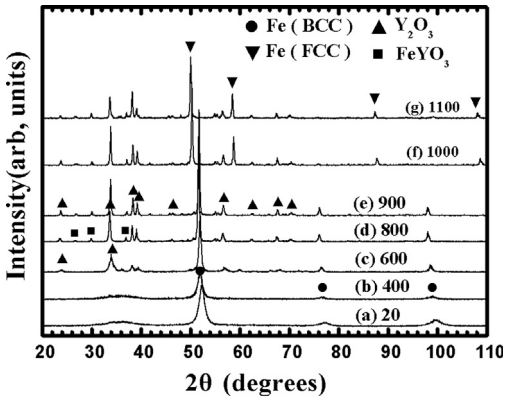


**Fig. 8** XRD patterns of the powders milled for 48 h and measured at different temperatures: (a) 20°C, (b) 400°C, (c) 600°C, (d) 800°C, (e) 900°C, (f) 1000°C and (g) 1100 °C.

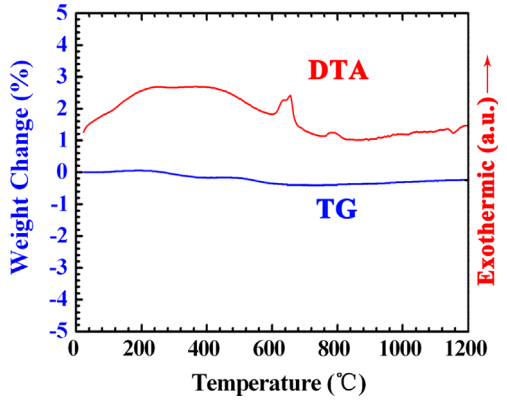


**Fig. 9** TG-DTA analysis of the Fe-25 wt% $Y_2O_3$ powders milled for 48 h.

boundaries, which are of low energy areas, and the nanocrystalline $Y_2O_3$ changes into amorphous structure and is inclined to stay at these grain boundaries.

Fig. 8 shows the XRD patterns of Fe-25 wt% $Y_2O_3$ powders milled for 48 h and measured in situ at different temperatures. It can be seen from Fig. 8(a) and (b) that as compared with the amorphous structure of the as-milled powders, $Y_2O_3$ in the powders annealed at 400 °C still keeps the amorphous structure with a broad diffuse peak between 30° and 40°. The powders measured at 600 °C exhibit the diffraction peaks at about 23.8°, 34.0°, 38.1°, 39.8°, 57.1° and 68.1°, indicating that $Y_2O_3$ start to nucleate into crystalline status. Fig. 9 shows TG-DTA thermal analysis curves of Fe-25 wt% $Y_2O_3$ powders milled for 48 h. An obvious exothermic peak near 620 °C is recognized with a starting temperature of 600 °C. This demonstrates that the crystallization of $Y_2O_3$ happens at 600 °C. When the in situ measuring temperature reaches 800 °C, the intensity of the diffraction peaks $Y_2O_3$ in Fig. 8(d) increases and the width of the diffraction peaks decreases due to the growth of $Y_2O_3$ nanocrystals during annealing. Meanwhile, three weak XRD peaks at 26.4°, 30.2° and 37.3° of crystalline $FeYO_3$ are also observed in Fig. 8(d), which is also proved by the exothermic peak in the vicinity of 800 °C in Fig. 9. These results confirm that the original amorphous oxide also contains a small amount of Fe, although the Y and O are the dominant elements in the amorphous oxide. The solid-state amorphization process can be expressed as $Y_2O_3 + Fe \rightarrow Y - Fe - O$ (amorphous). The crystallization process during annealing can be expressed as $Y - Fe - O$ (amorphous) $\rightarrow Y_2O_3 + YFeO_3$. The XRD pattern of the powders annealed at 900 °C reveals no remarkable changes as compared with the powders annealed at 800 °C. It can be seen from Fig. 8(f) and (g) that when the measuring temperature is above 1000 °C, the diffraction peaks of γ-Fe occurred due to the phase transition from α-Fe to γ-Fe.

## 4. Conclusions

The microstructural evolution of $Y_2O_3$ nanoparticles and matrix α-Fe in Fe-25 wt% $Y_2O_3$ powders during MM and annealing was clarified. All the elements distribute homogenously inside the powders after 48 h of MM. The lattice constant of matrix α-Fe keeps constant with milling time, indicating that no solid solution takes place during MM process. The mean particle size and crystalline size of MM powders decrease with milling time and reach a saturation value at 48 h. After 8 h of MM, the α-Fe in each powder becomes nanocrystalline. After 48 h of MM, $Y_2O_3$ changes from nanostructure into amorphous structure and the crystalline size of α-Fe is further decreased to 10 nm. The $Y_2O_3$ in the powders mechanically milled for 48 h keeps the amorphous structure after annealing at 400 °C, and starts to crystallize when the powders are annealed at 600 °C. The amorphous $Y_2O_3$ contains a small amount of Fe, and crystalline $FeYO_3$ appears at 800 °C.

## Acknowledgments

The authors acknowledge the support of this work by MOST of China (No. 2013CB035503), the Aeronautical Science Foundation of China (No. 2011ZF51065), the Specialized Research Fund for the Doctoral Program of Higher Education (No. 20091102120009), and the Scientific Research Foundation for the Returned Overseas Chinese Scholars, State Education Ministry. We also thank

Professor Huiping Duan and Center for Instrumental Analysis and Research, Beihang University for the technical aid in TEM observation.

## References

[1] J.S. Benjamin, Scientific American 234 (1976) 40–48.
[2] C. Suryanarayana, Progress in Materials Science 46 (2001) 1–184.
[3] J.S. Benjamin, Metallurgical Transactions 1 (1970) 2943–2951.
[4] J.S. Benjamin, M.J. Bomford, Metallurgical Transactions 5 (1974) 615–621.
[5] L.J. Park, H.J. Ryu, S.H. Hong, Y.G. Kim, Advanced Performance Materials 5 (1998) 279–290.
[6] M. Turker, T.A. Hughes, Oxidation of Metals 44 (1995) 505–525.
[7] R. Leholm, B. Norris, A. Gurney, Advanced Materials and Processes (USA) 159 (2001) 27–31.
[8] R.W. Grimes, W.J. Nuttall, Science 329 (2010) 799–803.
[9] G.R. Odette, M.J. Alinger, B.D. Wirth, Annual Review of Materials Research 38 (2008) 471–503.
[10] I. Charit, K.L. Murty, Journal of Operations Management 62 (2010) 67–74.
[11] J.H. Weber, R.K. Wilson, Materials Design Approaches and Experiences as Held during the TMS Fall Meeting, Indianapolis, USA, 2001, pp. 97–109.
[12] M.A. Munoz-Morris, C.G. Oca, D.G. Morris, Acta Materialia 51 (2003) 5187–5197.
[13] M.A. Miodownik, A.J. Wilkinson, J.W. Martin, Acta Materialia 46 (1998) 2809–2821.
[14] H.R.Z. Sandim, A.O.F. Hayama, D. Raabe., Materials Science and Engineering A 430 (2006) 172–178.
[15] P. Susila, D. Sturm, M. Heilmaier, B.S. Murty, V.S. Sarma, Materials Science and Engineering A 528 (2011) 4579–4584.
[16] M. Li, Z.J. Zhou, P. He, Y.L. Xu, L. Liao, Journal of Nuclear Materials 417 (2011) 189–192.
[17] A. Daoud, J.B. Vogt, E. Charkaluk, J. Bouquerel, L. Zhang, J.C. Biasci, Materials Science and Engineering A 534 (2012) 640–648.
[18] L. Zhang, X.H. Qu, X.B. He, R. Din, M.L. Qin, H.M. Zhu, Journal of Alloys and Compounds 512 (2012) 39–46.
[19] M.A. Montealegre, J.L. Gonzalez-Carrasco, M.A. Morris-Munoz, J. Chao, D.G. Morris, Intermetallics 8 (2000) 439–446.
[20] J.L. Gonzalez-Carrasco, P. Perez, P. Adeva, J. Chao, Intermetallics 7 (1999) 69–78.
[21] Y. Kimura, S. Takaki, S. Suejima, R. Uemor, H. Tamehiro, ISIJ International 39 (1999) 176–182.
[22] T. Okuda, M. Fujiwara, Journal of Materials Science Letters 14 (1995) 1600–1603.
[23] C.C. Eiselt, M. Klimenkov, R. Lindau, A. Moslang, H.R.Z. Sandim, A.F. Padilha, D. Raabe, Journal of Nuclear Materials 385 (2009) 231–235.
[24] V. Castro, T. Leguey, A. Munoz, M.A. Monge, R. Pareja, E.A. Marquis, S. Lozano-Perez, M.L. Jenkins, Journal of Nuclear Materials (386–388) (2009) 449–452.
[25] K. Omuro, H. Miura, Applied Physics Letters 60 (1992) 1433–1435.
[26] L. Aymard, A. Delahaye-Vidal, F. Portemer, F. Disma, Journal of Alloys and Compounds 238 (1996) 116–127.
[27] J.Z. Jiang, F.W. Poulsen, S. Morup, Journal of Materials Research 14 (1999) 1343–1352.
[28] L. Dai, Y.C. Liu, Z.Z. Dong, Powder Technology 217 (2012) 281–287.